JOURNAL OF COMPUTATIONAL PHYSICS **138,** 480–500 (1997)
ARTICLE NO. CP975827

Hybrid Ray–FDTD Moving Window Approach to Pulse Propagation

B. Fidel,* E. Heyman,* R. Kastner,* and R. W. Ziolkowski†

**Faculty of Engineering, Department of Electrical Engineering-Physical Electronics, Tel-Aviv University, Tel-Aviv 69978, Israel; and †Department of Electrical and Computer Engineering, University of Arizona, Tucson, Arizona 85721*

Received February 15, 1995; revised May 23, 1996

A moving window finite difference time domain method is developed to simulate the propagation of electromagnetic pulses over large distances. Both Eulerian and Lagrangian approaches to solving Maxwell's equations in a moving window are obtained and contrasted. The Lagrangian approach is shown to be superior for electromagnetic pulse propagation; it is demonstrated that dispersion-free numerical propagation can be achieved with the Lagrangian approach. Examples of propagation in homogeneous and inhomogeneous media, and scattering from a interface between two media are considered. The scattering results are achieved with a window splitting approach in which the original incident pulse window is frozen at the interface and new windows are generated after the interface interactions occur that move with the reflected and transmitted pulses. The simulation results are shown to be accurate and physically appealing.

I. INTRODUCTION

This paper describes our initial efforts in the development of an efficient and accurate numerical approach for modeling the propagation of localized wavepackets in complex environments over large distances. Several classes of such solutions of the time-dependent scalar wave and vector Maxwell equations have been introduced recently in linear and in nonlinear media. The major difficulties in modeling such long distance propagation problems with an explicit, discrete numerical approach are the vast computer resources needed to discretize the entire region of interest and the accumulation of numerical dispersion error. Furthermore, these difficulties tend to reinforce each other. The numerical dispersion can be reduced by using a finer grid; i.e., a finer grid would maintain a prescribed level of dispersion error.

0021-9991/97 $25.00

Unfortunately, this quickly exhausts the available computer resources when large propagation distances are desired.

As will be described in this paper, we have developed a hybrid method that combines two well-known modeling approaches: the asymptotic ray technique and the discrete, finite difference time domain (FDTD) method, to overcome these difficulties. The current study emphasizes a one-dimensional realization of the general concept. This will allow us to introduce the basic ideas of this modeling approach, illustrate its properties, and validate its effectiveness against well-known results. Nonetheless, it also provides us a means to illustrate our long-term goal which is to treat fully three-dimensional propagation environments.

For the three-dimensional space-time wavepackets mentioned above, it has been shown recently that they remain localized and propagate with the local wave speed along the characteristic ray trajectories of the medium [1]. The propagation trajectory in these problems can be determined *a priori* by solving the corresponding ray equation subject to the appropriate initial conditions. A moving window which encompasses this wavepacket can be constructed by first solving the ray trajectories subject to the appropriate initial conditions and then describing the local field by means of the transformation

$$\vec{E}(\mathbf{r}, t) \to \vec{E}\left(\mathbf{r}, t - \int^{\sigma} \frac{d\sigma}{c_0(\sigma)}\right), \tag{1.1}$$

where the integration accounts for the ''geometrical'' propagation delay along the ray trajectory, the terms σ and c_0 being, respectively, the arc length and the wave speed along the ray. Using the transformation in (1.1) to define the window and centering the center-of-mass of the wavepacket in it, the FDTD grid is progressively updated as the wavepacket propagates. The associated dynamics of the window need to be determined, either analytically *a priori* or numerically as the computation progresses. As the wavepacket propagates, its support changes both temporally and spatially due to dispersion and diffraction phenomena. These properties affect the window and cell size, as well as the space-time trajectory of the window's center of mass. One can model accurately its field structure with the FDTD approach in this local environment. The resulting moving window method (the envisioned three-dimensional concept is depicted in Fig. 1) combines the globally (large distance) defined rays with the local discrete methods. It would allow for local window refinements in regions of interest, for example, the main support of the wavepacket, so that the available memory can be spent on modeling where the action is rather than wastefully where it is not. As such, it provides a computationally efficient way for controlling the numerical dispersion errors which are critical for modeling any long distance wavepacket effects.

To model the wave interaction with complex structures with abrupt transitions such as the boundaries (interfaces) between two media, it will be shown that it is necessary to switch to a stationary FDTD window that properly models the local environment when the wavepacket is interacting with these discontinuities. A field will be re-radiated from these interactions; the resulting field must then be tracked along its own ray trajectory with its own moving FDTD window. In the interface

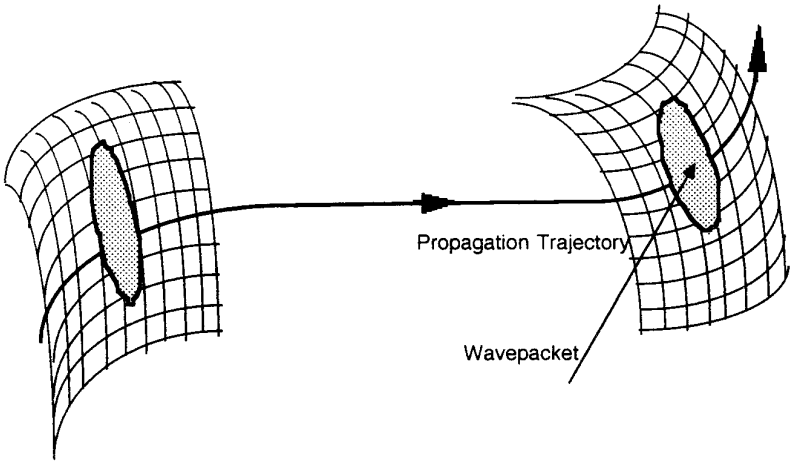

FIG. 1. The moving window approach for a wavepacket propagation along ray trajectory.

case, the reflected and transmitted fields will be tracked with independent moving FDTD windows, respectively, along the reflected and transmitted rays once the scattered field has split into these two independent component wavepackets. For gradual transitions it must be realized that there will be continual leakage of the reflected wave energy out the back of the moving window. Even though the forward propagating wave energy is captured by this scheme, it is not possible to capture this backward propagating wave energy in a finite window. Consequently we restrict our development either to slowly varying media or media with abrupt transitions. In this paper we clarify the proposed approach by considering the propagation of a localized wavepacket in such one-dimensional homogeneous and inhomogeneous media.

Several alternative moving window formulations are presented for our one-dimensional test problem, viz., normal propagation of a pulsed plane electromagnetic wave in a planar stratified medium. We use a short excitation pulse and track the field within an FDTD window specified by the moving frame transformation (1.1) which is determined by the local propagation speed in the medium. The motivation for this problem choice is the desire to clarify the efficiency and accuracy of the moving window formulation. The effect of the moving window boundary condition and the method for generating the independent local FDTD windows during an interface interaction will be emphasized. We also closely examine different approaches for reducing the numerical dispersion. As mentioned above, by restricting the window to the region where the pulse is located, we are able to use fine discretization steps while tracking the field to very large distances. However, in order to reduce these dispersion errors further, we also introduce a coordinate transformation that results in a moving coordinate system which is stationary relative to the pulse. Even though the standard methods incur large dispersion errors, we will demonstrate that when this transformed Maxwell's equation system, termed here the Lagrange formulation, is discretized, the resulting simulations produce dispersion-free numerical propagation for the forward propagating pulse.

II. ALTERNATIVE MOVING WINDOW FORMULATIONS

The moving window concept is designed to facilitate the modeling of the propagation of pulses over long ranges. In this process, a number of sources for errors must be considered, and the means to control them developed. The most notable error arising in long range propagation stems from numerical dispersion. Nonetheless, effects which lead to instabilities and reduced computational efficiencies are also of great importance. These errors will have different impacts on the results depending on the specific formulation used for the moving window equations.

Two principal options have been considered for the moving FDTD windows, viz., a stationary and a moving coordinate system. In the first option, an Eulerian approach, Maxwell's continuous equations are applied in the stationary coordinate space over a different spatial region at each time step. The resulting moving FDTD window travels along with the center-of-mass of the pulse in the stationary coordinate space. Alternatively, the moving FDTD window can be attached to a moving coordinate system and, hence, is stationary with respect to this center-of-mass system. This Lagrange approach requires a suitable transformation of the field equations, as shown below. These Lagrange modified field equations exhibit markedly different properties from their Eulerian or standard discretization counterparts.

II.A. *Euler's Formulation: A Moving Window in a Stationary Coordinate Frame*

As mentioned in the Introduction, we consider the problem of normal propagation of a plane electromagnetic wave in a plane stratified medium identified by the permittivity, $\varepsilon(z)$, and the permeability, $\mu(z)$, of the medium. We assume (without loss of generality) that the field is x-polarized. The Maxwell curl equations in one space dimension and time are expressed as

$$\frac{\partial H_y}{\partial t} = -\frac{c(z)}{Z(z)}\frac{\partial E_x}{\partial z}, \qquad \frac{\partial E_x}{\partial t} = -c(z)Z(z)\frac{\partial H_y}{\partial z}, \tag{2.1}$$

where we introduce, respectively, the wave speed and wave impedance

$$c(z) = 1/\sqrt{\varepsilon\mu}, \qquad Z(z) = \sqrt{\mu/\varepsilon}. \tag{2.2}$$

This set of equations has a convenient one-dimensional telegrapher equation form. Henceforth we shall omit from the field components the coordinate labeling indices x and y. We note that this model problem contains no conductivity or other dispersive effects in the medium in order to simplify the discussion and to isolate the numerical dispersion effects, which will be discussed in detail below.

The field equations are discretized in the standard FDTD staggered grid, leapfrog algorithm form [1, 2] as

$$\begin{aligned} H_{i+1/2}^{n+1/2} &= H_{i+1/2}^{n-1/2} - \frac{\Delta t}{\Delta z}\frac{c_{i+1/2}}{Z_{i+1/2}}(E_{i+1}^{n} - E_i^n) \\ E_i^{n+1} &= E_i^n - \frac{\Delta t}{\Delta z} c_i Z_i (H_{i+1/2}^{n+1/2} - H_{i-1/2}^{n+1/2}), \end{aligned} \tag{2.3}$$

where, for instance, $H_{i+1/2}^{n+1/2}$ represents the magnetic field sampled at the space point $(i + 1/2)\,\Delta z$ at the time $(n + 1/2)\,\Delta t$. This interleaved field-component, space-time approach generates second-order accurate numerical simulations.

1. *Stability analysis.* In order to avoid instability problems with this standard FDTD algorithm, it is well known [3] that the space and time steps must obey the Courant–Friedrichs–Lewy (CFL) condition. Below we shall present a derivation of this condition which is similar to the one given in [2, 3] but extended to nonuniform media. It will also be used in the alternative formulations considered in subsequent sections.

In order to construct a transition matrix between the discrete field values at a given point z_i for consecutive time steps, we base the analysis on the following ansatz for *a spatial harmonic solution* of (2.3)

$$H_{i+1/2}^{n+1/2} = \mathscr{H}_{i+1/2}^{n+1/2} e^{ikz_{i+1/2}}, \qquad E_i^n = \mathscr{E}_i^n e^{ikz_i}, \tag{2.4}$$

where the envelope functions $\mathscr{H}_i^n(k)$ and $\mathscr{E}_i^n(k)$ are slowly varying functions of i but have unrestricted variation with n, i.e.,

$$\left| \frac{\mathscr{E}_{i+1}^n - \mathscr{E}_i^n}{\mathscr{E}_i^n} \right| \ll 2 \sin K/2 \tag{2.5}$$

with $K = k\,\Delta z$. Substituting (2.4) in (2.3) and using (2.5), we obtain

$$\mathscr{H}_{i+1/2}^{n+1/2} = \mathscr{H}_{i+1/2}^{n-1/2} - i2 \frac{\Delta t}{\Delta z} \frac{c_{i+1/2}}{Z_{i+1/2}} \mathscr{E}_i^n \sin K/2 \tag{2.6}$$

$$\mathscr{E}_i^{n+1} = \mathscr{E}_i^n - i2 \frac{\Delta t}{\Delta z} c_i Z_i \mathscr{H}_{i+1/2}^{n+1/2} \sin K/2. \tag{2.7}$$

Substitution of (2.6) into (2.7) results in the expression

$$\mathscr{E}_i^{n+1} = \mathscr{E}_i^n \left[1 - 4 \left(\frac{\Delta t}{\Delta z} \right)^2 c_i c_{i+1/2} \frac{Z_i}{Z_{i+1/2}} \sin^2 K/2 \right] - i2 \frac{\Delta t}{\Delta z} c_i Z_i \mathscr{H}_{i+1/2}^{n-1/2} \sin K/2. \tag{2.8}$$

Since c and Z are slowly varying functions on the scale of Δz, this expression may be simplified by using, to first order, $c_{i+1/2} \simeq c_i(1 + \frac{1}{2}\,\Delta z \ln' c_i)$ where $\ln' c = c'/c$ and the prime denotes a derivative with respect to z. A similar approximation applies for Z. However, since the variations of the envelope functions $\mathscr{E}_i^n$ and $\mathscr{H}_i^n$ as functions of i are typically proportional to the variation of c_i (e.g., see the WKB solution in (3.5) below), it follows that, to the same order of approximation, we may use $c_{i+1/2} \simeq c_i$ and $Z_{i+1/2} \simeq Z_i$. Equations (2.6) and (2.8) can thus be combined in the concise form

$$\begin{pmatrix} \mathscr{H}_{i+1/2}^{n+1/2} \\ \mathscr{E}_i^{n+1} \end{pmatrix} = \mathbf{T}_i \begin{pmatrix} \mathscr{H}_{i+1/2}^{n-1/2} \\ \mathscr{E}_i^n \end{pmatrix}, \tag{2.9}$$

where the transition matrix is

$$\mathbf{T}_i = \begin{pmatrix} 1 & -i2\gamma_i Z_i^{-1} \sin K/2 \\ -i2\gamma_i Z_i \sin K/2 & 1 - 4\gamma_i^2 \sin^2 K/2 \end{pmatrix} \tag{2.10}$$

and we use $\gamma_i = c_i\, \Delta t/\Delta z$. The eigenvalues of this matrix are

$$g = 1 - 2\gamma_i^2 \sin^2(K/2) \pm i2\gamma_i \sin(K/2)\sqrt{1 - \gamma_i^2 \sin^2(K/2)}. \tag{2.11}$$

In order for the formulation to be stable, the condition $gg^* \leq 1$ must be satisfied for *both* eigenvalues. One may show that this condition is satisfied only if $\gamma_i^2 \sin^2 K/2 < 1$ in (2.11) (in which case $|g| = 1$). Applying this condition for any K, it follows that the space and time steps must obey the CFL condition

$$\gamma(z) \equiv c(z)\frac{\Delta t}{\Delta z} \leq c_{\max}\frac{\Delta t}{\Delta z} < 1. \tag{2.12}$$

2. *Numerical dispersion.* The numerical dispersion relation is obtained by assuming *a space and time harmonic solution* of the form

$$H_{i+1/2}^{n+1/2} = \tilde{\mathscr{H}}_{i+1/2}^{n+1/2} e^{-i(\omega t_{n+1/2} - kz_{i+1/2})}, \qquad E_i^n = \tilde{\mathscr{E}}_i^n e^{-i(\omega t_n - kz_i)}, \tag{2.13}$$

where the envelope functions $\tilde{\mathscr{H}}_{i+1/2}^{n+1/2}(\omega, k)$ and $\tilde{\mathscr{E}}_i^n(\omega, k)$ are slowly varying functions of i and n, i.e., they satisfy (cf. (2.5))

$$\left|\frac{\tilde{\mathscr{E}}_{i+1}^n - \tilde{\mathscr{E}}_i^n}{\tilde{\mathscr{E}}_i^n}\right| \ll 2 \sin K/2, \qquad \left|\frac{\tilde{\mathscr{E}}_i^{n+1} - \tilde{\mathscr{E}}_i^n}{\tilde{\mathscr{E}}_i^n}\right| \ll 2 \sin \Omega/2, \tag{2.14}$$

where $\Omega = \omega\, \Delta t$. Substituting (2.13) into (2.3) and using (2.14), we obtain the matrix equation

$$\begin{pmatrix} -\sin \Omega/2 & \gamma_i Z_i^{-1} \sin K/2 \\ -\gamma_i Z_i \sin K/2 & \sin \Omega/2 \end{pmatrix} \begin{pmatrix} \tilde{\mathscr{H}}_{i+1/2}^{n+1/2} \\ \tilde{\mathscr{E}}_i^n \end{pmatrix} = 0. \tag{2.15}$$

A solution of (2.15) requires the determinant to be zero, yielding the well-known dispersion relationship

$$\sin^2 \Omega/2 = \gamma^2(z) \sin^2 K/2. \tag{2.16}$$

The numerical group velocity is then inferred from this numerical dispersion relationship; it has the form

$$v_g(z) \equiv \frac{\partial \omega}{\partial k} = \frac{c(z)\sqrt{1 - \gamma^{-2}(z) \sin^2 \Omega/2}}{\cos \Omega/2} \simeq c\left[1 - \frac{1}{8}\Omega^2(\gamma^{-2} - 1)\right]. \tag{2.17}$$

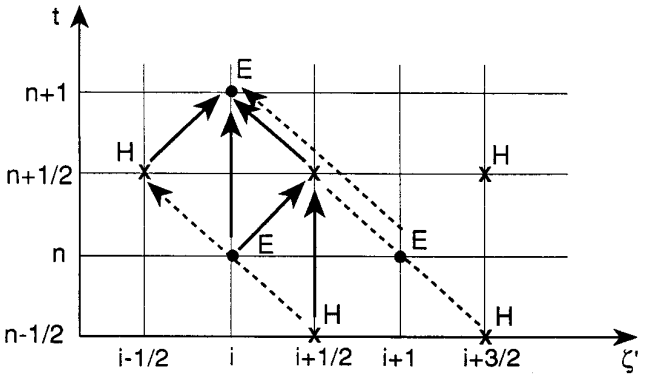

FIG. 2. The FDTD stencil. The full and dashed line arrows indicate, respectively, FDTD integrations and window shifts.

In this relation ω is taken as a typical frequency parameter in the pulse. The approximate expression in (2.17), which applies if $\Omega \ll 1$, explains implicitly how the dispersion errors grows for $\gamma < 1$. Curves of the group velocity will be considered in Section III, together with a thorough analysis of the long distance effects of any errors in the numerical group velocity.

3. *Discussions: Limitations of the global uniform grid approach.* Applying the standard FDTD formulation, one must invoke the stationary equations (2.3) over a finite grid at each time step. In the Eulerian approach the discrete Maxwell's equations are the same as (2.3). However, the grid is now arranged to be centered about the pulse location; this moving window is achieved at each time step by deleting the necessary number of trailing-edge grid points from this window and then adding an appropriate number of samples at the leading edge of the window. The field quantities are assumed to be small in these regions to make this process effective. The unknown field quantities are then updated in the standard manner; an appropriate radiating boundary condition is specified at all boundaries. Note that one may view this formulation as having a large stationary grid from which only a small group of selected samples which is centered about the pulse location is highlighted by the moving window at each time step. Following the updating process, the indices of all the sampled quantities are shifted to allow for the same set of indices at each time step; however, this shift is not an essential process in the stationary formulation. Figure 2 shows the transformation of indices within the FDTD stencil as a result of both the integration of (2.3) and the subsequent shift of indices.

When applying this straightforward formulation to a one-dimensional inhomogeneous medium with wave speed $c(z)$ and wave impedance $Z(z)$, one may note that the CFL condition (2.12) needs to be determined by the point at which the medium wave speed is the highest and γ is close to the limit $\gamma \to 1$. At points where $c \ll c_{\max}$, γ may become much smaller; and the overall numerical efficiency will be severely reduced, particularly if there is only a small region where $c \sim c_{\max}$. On the other hand, as will be discussed below, setting the CFL condition to its maximum

value will cause an accumulated numerical dispersion effect over long range propagation (see (2.17)). This conflict of optimal choices results in the need to carefully select the appropriate value for the CFL condition.

II.B. *Euler's Formulation: A Moving Grid in a Speed-Normalized Coordinate Frame*

In order to alleviate these problems, a modification of the stationary grid formulation is introduced. Instead of using constant space and time steps Δz and Δt, (2.1) is modified to accommodate an optical length coordinate

$$\zeta(z) = \int_0^z \frac{c_0}{c(z')}\, dz', \tag{2.18}$$

where c_0 is an arbitrary constant reference velocity. The time steps and the optical path length are then sampled uniformly. This renders the spatial grid nonuniform, with Δz now being proportional to $c(z)^{-1}$, while the propagation times between any two adjacent grid points along z remain the same.

The continuous equations become

$$\frac{\partial H}{\partial t} = -\frac{c_0}{Z(z)}\frac{\partial E}{\partial \zeta}, \qquad \frac{\partial E}{\partial t} = -c_0 Z(z)\frac{\partial H}{\partial \zeta} \tag{2.19}$$

and are discretized as follows:

$$\begin{aligned} H_{i+1/2}^{n+1/2} &= H_{i+1/2}^{n-1/2} - \frac{\Delta t}{\Delta \zeta}\frac{c_0}{Z_{i+1/2}}\left(E_{i+1}^{n} - E_i^n\right) \\ E_i^{n+1} &= E_i^n - \frac{\Delta t}{\Delta \zeta} c_0 Z_i \left(H_{i+1/2}^{n+1/2} - H_{i-1/2}^{n+1/2}\right). \end{aligned} \tag{2.20}$$

By comparing (2.1)–(2.3) with (2.19)–(2.20) it follows that the analysis of the speed-normalized coordinate frame is identical with that of the uniform Δz approach, presented in Section II.A, with the replacement $z \to \zeta$ and $c(z) \to c_0 = \text{const}$. Specifically the modified CFL condition becomes (cf. (2.12))

$$\gamma_0 \equiv c_0 \frac{\Delta t}{\Delta \zeta} \leq 1. \tag{2.21}$$

Thus, unlike the uniform Δz approach, the speed-normalized parameterization ensures that γ is a fixed constant over the entire domain. One can then set $\gamma_0 = 1$ for the sake of efficiency and, as shown below, for reduced numerical dispersion.

Likewise, the dispersion relation for this speed-normalized coordinate Euler representation becomes (cf. (2.16))

$$\sin^2 \Omega/2 = \gamma_0^2 \sin^2 K/2, \tag{2.22}$$

where $\Omega = \omega\, \Delta t$ and $K = k\, \Delta \zeta$. The numerical group velocity v_g is given therefore

by (2.17) with the replacements $c(z) \to c_0$ and $\gamma(z) \to \gamma_0$. Thus, unlike the uniform Δz approach, the speed-normalized approach ensures that the γ as well as the numerical group velocity are constants.

II.C. *The Lagrange Formulation: Moving Coordinate Frame*

Another formulation is possible and is developed by transforming Maxwell's equations to a coordinate frame that moves with the pulse. To achieve this Lagrange formulation, we transform to the public coordinate system

$$\begin{aligned} t' &= t \\ \zeta' &= \zeta(z) - c_0 t. \end{aligned} \tag{2.23}$$

The one-dimensional curl equations become

$$\frac{\partial H}{\partial t} = c_0 \frac{\partial H}{\partial \zeta'} - \frac{c_0}{Z(z)} \frac{\partial E}{\partial \zeta'}, \qquad \frac{\partial E}{\partial t} = c_0 \frac{\partial E}{\partial \zeta'} - c_0 Z(z) \frac{\partial H}{\partial \zeta'}. \tag{2.24}$$

One can show that (2.24) is equivalent to the following product of one-way wave equations in E,

$$\left(\frac{\partial}{\partial t}\right)\left(\frac{\partial}{\partial t} - 2c_0 \frac{\partial}{\partial \zeta'}\right) E = 0, \tag{2.25}$$

where the first and second operators are, respectively, the forward and backward "one-way wave operators" along the characteristics $dz/dt = \pm c(z)$. Equation (2.25) reveals the expected wave characteristics in the moving coordinate frame, i.e., in the absence of numerical dispersion waves will travel at speeds 0 or $-2c$ within the frame.

Because of possible numerical dispersion effects, it must be stressed that the introduction of the discrete equivalents of this system may not reproduce these characteristic speeds. It will be shown below that the Lagrange moving frame formulation reproduces the forward propagating characteristic $\partial_t E = 0$ without dispersion in contrast to the backward propagating characteristic.

Upon comparison of (2.24) with (2.1), we note that an extra spatial derivative of the quantity that appears with the time derivative is now present. While the shifted grid within the *conventional FDTD* approach of Yee [2] normally provides an efficient numerical description for the physics underlying Eqs. (2.19)–(2.20), it does not allow a straightforward implementation when a moving coordinate system (t, ζ') is included. Because the spatial derivative of H as well as that of E must be evaluated in Eqs. (2.24), the values of both H and E at the same time are required. This construct contradicts the underlying assumption of the staggered space-time grid approach [2] that these components be evaluated at different increments of the time step. For this reason, alternating grids for E and H as used in the Yee algorithm [2] are no longer desirable. Instead we must resort to sampling the field components at the same space-time locations, i.e., both E and H must be evaluated

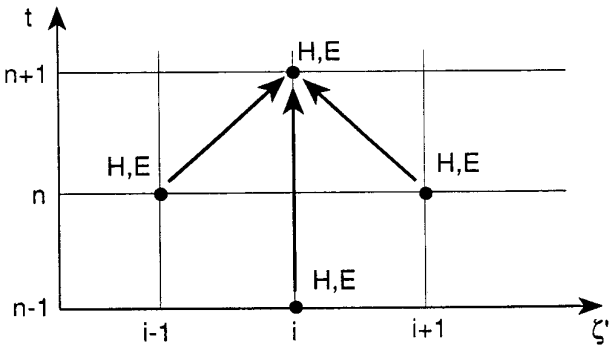

FIG. 3. The Lagrange FDTD stencil.

using the same grid points. The resulting Lagrange FDTD stencil is shown in Fig. 3. The discretized form of the Maxwell's equations set (2.24) is thus

$$\begin{aligned} H_i^{n+1} &= H_i^{n-1} + c_0 \frac{\Delta t}{\Delta \zeta'} (H_{i+1}^n - H_{i-1}^n) - \frac{\Delta t}{\Delta \zeta'} \frac{c_0}{Z_i^n} (E_{i+1}^n - E_{i-1}^n) \\ E_i^{n+1} &= E_i^{n-1} + c_0 \frac{\Delta t}{\Delta \zeta'} (E_{i+1}^n - E_{i-1}^n) - \frac{\Delta t}{\Delta \zeta'} c_0 Z_i^n (H_{i+1}^n - H_{i-1}^n). \end{aligned} \tag{2.26}$$

Note: The index n in Z^n does not imply that Z changes with time; rather, it represents the fact that the frame moves relative to the medium. In (2.26) both E and H occupy the same grid points as desired, the grids being uniform in t and ζ' with the increments Δt and $\Delta \zeta'$, respectively. The field components E and H are located at the points $i\,\Delta\zeta'$ and are updated at the increments of the time step, $n\,\Delta t$. The numerical scheme (2.26) results in second-order central differencing in space and time [4].

Using such a second-order differencing scheme in time requires knowledge of the E and H values at two previous time levels. For the initial time level, $t = 0$, we have the specified analytical initial conditions as given in (3.1) below. However, for the time instant $t = \Delta t$, the E and H values must be found by using a "boot-strapping" technique which utilizes a first-order in time, second-order in space Lax–Fredrichs scheme [4]. This latter scheme is used to advance the solution from $t = 0$ to $t = \Delta t/8$, i.e., it generates the values

$$\begin{aligned} H_i^{\Delta t/8} &= \frac{1}{2}(H_{i+1}^0 + H_{i-1}^0) + \frac{\Delta t}{16\Delta \zeta'}(H_{i+1}^0 - H_{i-1}^0) - \frac{c_0}{Z_i^0}\frac{\Delta t}{16\Delta \zeta'}(E_{i+1}^0 - E_{i-1}^0) \\ E_i^{\Delta t/8} &= \frac{1}{2}(E_{i+1}^0 + E_{i-1}^0) + c_0 \frac{\Delta t}{16\Delta \zeta'}(E_{i+1}^0 - E_{i-1}^0) - \frac{\Delta t}{16\Delta \zeta'} c_0 Z_i^0 (H_{i+1}^0 - H_{i-1}^0). \end{aligned} \tag{2.27}$$

The scheme (2.26) is then used to advance the solution from $t = \Delta t/8$ to $t = \Delta t/4$, from $t = \Delta t/4$ to $t = \Delta t/2$, and then from $t = \Delta t/2$ to $t = \Delta t$. Although the Lax–Fredrichs scheme is only first-order in time, the "boot-strapping" technique enables the overall accuracy of the scheme to be second-order in time.

1. *Stability analysis.* The stability criterion for this Lagrange approach is again derived via the transition matrix approach. Expressing the fields by the local "Fourier amplitudes" $\mathscr{H}_i^n$ and $\mathscr{E}_i^n$ as in (2.4), and rewriting (2.26) for these amplitudes, assuming that they are slowly varying functions of i in the manner of (2.5), we obtain

$$\begin{pmatrix} \mathscr{H}_i^{n+1} \\ \mathscr{E}_i^{n+1} \end{pmatrix} = \begin{pmatrix} \mathscr{H}_i^{n-1} \\ \mathscr{E}_i^{n-1} \end{pmatrix} + \begin{pmatrix} i2\gamma_0 \sin K' & -i2Z^{-1}(\zeta')\gamma_0 \sin K' \\ -i2Z(\zeta')\gamma_0 \sin K' & i2\gamma_0 \sin K' \end{pmatrix} \begin{pmatrix} \mathscr{H}_i^n \\ \mathscr{E}_i^n \end{pmatrix}, \tag{2.28}$$

where $K' = k\,\Delta\zeta'$. To bring this equation into the desired transition matrix form

$$\begin{pmatrix} \mathscr{H}_i^{n+1} \\ \mathscr{E}_i^{n+1} \end{pmatrix} = \mathbf{T} \begin{pmatrix} \mathscr{H}_i^{n} \\ \mathscr{E}_i^{n} \end{pmatrix} \tag{2.29}$$

we substitute in (2.28) the definition of the yet unknown eigenvalues g

$$\mathbf{T} \begin{pmatrix} \mathscr{H}_i^{n} \\ \mathscr{E}_i^{n} \end{pmatrix} = g \begin{pmatrix} \mathscr{H}_i^{n} \\ \mathscr{E}_i^{n} \end{pmatrix} \tag{2.30}$$

thereby obtaining

$$\mathbf{T} = \begin{pmatrix} i2\gamma_0 \sin K' + 1/g & -i2Z^{-1}(\zeta')\gamma_0 \sin K' \\ -i2Z(\zeta')\gamma_0 \sin K' & i2\gamma_0 \sin K' + 1/g \end{pmatrix}. \tag{2.31}$$

The characteristic equation for the eigenvalues g is therefore

$$\det \begin{vmatrix} i2\gamma_0 \sin K' + 1/g - g & -i2Z^{-1}(\zeta')\gamma_0 \sin K' \\ -i2Z(\zeta')\gamma_0 \sin K' & i2\gamma_0 \sin K' + 1/g - g \end{vmatrix} = 0; \tag{2.32}$$

hence the eigenvalues are

$$g = i2\gamma_0 \sin K' \pm \sqrt{1 - 4\gamma_0^2 \sin^2 K'}. \tag{2.33}$$

Again, the condition $gg^* \leq 1$ is satisfied only if $4\gamma_0^2 \sin^2 K' \leq 1$ (in which case $|g| = 1$). Consequently, the following modified CFL criterion results:

$$\Delta t \leq \frac{\Delta\zeta'}{2c_0}. \tag{2.34}$$

Note that $2c_0$ factor in this criterion as compared with the stationary coordinate criterion (2.21). This is due to the fact that the largest velocity in the Lagrange system is $2c_0$ (see (2.38)–(2.40)).

2. *Numerical dispersion.* To derive the numerical dispersion relation associated

with this discretized Lagrange formulation, we express the fields by their local "Fourier amplitudes" as in (2.13). Assuming that these amplitudes are slowly varying functions of i and n as in (2.5) and (2.14), we obtain (cf. (2.28))

$$\begin{pmatrix} i2(\gamma_0 \sin K' + \sin \Omega') & -i2Z^{-1}(\zeta')\gamma_0 \sin K' \\ -i2Z(\zeta')\gamma_0 \sin K' & i2(\gamma_0 \sin K' + \sin \Omega') \end{pmatrix} \begin{pmatrix} \tilde{\mathscr{H}}_i^n \\ \tilde{\mathscr{E}}_i^n \end{pmatrix} = 0, \tag{2.35}$$

where $\Omega' = \omega\, \Delta t$. The local numerical dispersion relation is given therefore by

$$(\sin \Omega' + \gamma_0 \sin K')^2 = \gamma_0^2 \sin^2 K'. \tag{2.36}$$

For the numerical phase and group velocities, two solutions can be derived from (2.36). One solution for the forward propagating wave is simply

$$\sin \Omega' = 0 \Rightarrow v_g = v_p = 0. \tag{2.37}$$

This solution implies *the Lagrange formulation of the moving window method in one dimension is free of numerical dispersion* for this wave. It should be stressed that dispersion-free propagation is observed for the numerical implementation of (2.24) in its entirety, rather than exploiting only $\partial_t E = 0$. As the window moves along with the moving frame in an arbitrary medium, no numerical dispersion errors are observed. The relative numerical velocities of the pulse with respect to the observer are identically zero for all frequencies. This feature of the Lagrange formulation provides the means to ensure that long range propagation is indeed possible with little buildup of numerical dispersion errors.

The other solution applies to the backward propagating wave

$$\sin \Omega' = -2\gamma_0 \sin K' \tag{2.38}$$

giving

$$v_p = -\frac{c_0 \sin^{-1}(2\gamma_0 \sin K')}{\gamma_0 K'} \tag{2.39}$$

$$v_g = -\frac{2c_0 \cos K'}{\sqrt{1 - 4\gamma_0^2 \sin^2 K'}}. \tag{2.40}$$

For small $K' = k\, \Delta\zeta'$, the numerical group and phase velocities are approximately equal to $-2c_0$, as can be expected from (2.25) for the backward propagating wave in the moving window. For this component, the numerical dispersion error may become quite large. It also affects the modified CFL condition as noted in (2.34). However, the moving window concept is designed to track only forward propagating waves, letting local reflections exit the window as they propagate in the direction opposite to that of the window. Hence, they are not represented in the solution, and the numerical errors associated with them have no effect on the forward propagating pulse.

If, on the other hand, the solution involves both forward and backward propagat-

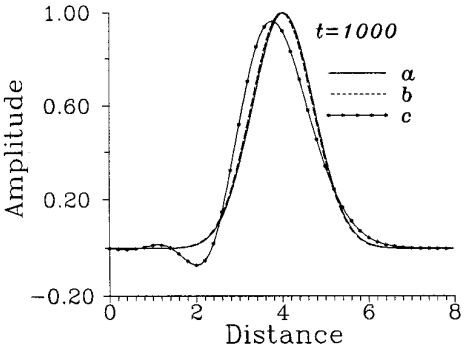

FIG. 4. Gaussian pulse propagation in a homogeneous medium with $c_0 = 1$. Observation time $t = 1000$ (equivalent to 1000 pulse lengths). Line (a): Exact solution. Line (b): Numerical moving window solutions for $\gamma = 1$ with $\Delta z = 0.02$ and for $\gamma = 0.5$ with $\Delta z = 0.005$ (both solutions are indistinguishable within the figure scale). Line (c): Numerical moving window solutions for $\gamma = 0.5$ with $\Delta z = 0.02$.

ing pulses, say due to a local abrupt discontinuity in the medium, then of course one should use two (or more) windows. Each window should track one propagating pulse in its own coordinate frame. Following the discussion above, the transformation to the pulse coordinate frame eliminates the numerical dispersion in the principal propagation direction of each pulse.

Other formulations are possible for the moving frame of reference. These formulations include those that employ a suitable change of variables of the form $E \to \overline{E}/Z(z)$ or $H \to \overline{H}Z(z)$. We have treated some of these schemes but found them to have regions of severe instabilities. Moreover, their accuracies were not as high as the schemes we are discussing in detail here. These alternates were not pursued further.

III. NUMERICAL RESULTS FOR LONG RANGE PROPAGATION

To explore the properties of the alternative moving grid formulations we have considered the problem of propagation of a Gaussian pulse in both a uniform and a layered media. The pulse is specified by the initial conditions

$$E(z,t)_{t=0} = f(z), \qquad H(z,t)|_{t=0} = \frac{1}{Z(z)} f(z), \tag{3.1}$$

where f is a Gaussian pulse

$$f(z) = \exp[-z^2/2(c_0 T)^2]. \tag{3.2}$$

For convenience we will use here normalized space and time coordinates so that $c_0 = 1$ and $T = 1$. The frequency spectrum of this pulse is bounded effectively by $|\omega| < 2$ or $|f| < 0.318$. A discretization step $\Delta z = 0.05$ therefore provides a $\sim\lambda/6$ discretization at the upper frequency range.

The effect of numerical dispersion in the Euler formulation in free space is demonstrated in Fig. 4 which shows the pulse within the moving window at $t =$

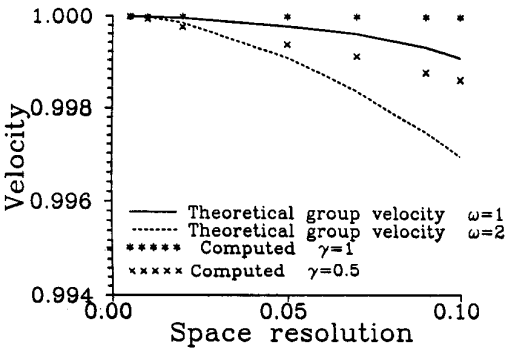

FIG. 5. Numerical dispersion characteristics for the Euler formulation. The solid and dashed lines are the theoretical group velocities at two typical frequencies $\omega = 1$, 1.2, and 2.0 with $\gamma = 0.5$. The crosses and the stars show the velocities of the numerical solutions of Fig. 4 for $\gamma = 0.5$ and $\gamma = 1$, respectively.

1000, i.e., at a distance equal to 1000 pulse widths from $z = 0$ for several choices of Δz and γ. Since the coordinate system is stationary as in the customary FDTD scheme, we anticipate that there will be no numerical dispersion when $\gamma = 1$. Indeed, the best agreement with the exact solution is obtained when $\gamma \to 1$, where from (2.36), theoretically no numerical dispersion is present, even for the relatively coarse sampling interval $\Delta z = 0.02$. When γ is reduced to 0.5, keeping Δz unchanged, a larger numerical dispersion error is experienced. This numerical dispersion error can then be reduced for smaller γ if a smaller Δz is specified. Indeed, using $\Delta z = 0.005$, with $\gamma = 0.5$ virtually eliminates the numerical dispersion effect for $t = 1000$.

The numerical dispersion characteristics for the Euler formulation in free space are verified in Fig. 5, where the computed pulse velocity is compared to the numerical group velocity (2.17). The theoretical group velocity is calculated at three typical frequencies: $\omega = 1$, 1.2, and 2.0, and for $\gamma = 0.5$. The results are thus depicted as functions of Δz. Also shown is the limiting case $\gamma = 1$ wherein $v_g = 1$. Note that the theoretical curves have the parabolic behavior described in (2.17). The computed pulse velocity for $\gamma = 0.5$ follows closely the theoretical curve with $\omega = 1.2$; and as such, it provides the explanation for the delay in the computed results when they are compared with the exact result in Fig. 4.

It is appropriate now to assess the effect of the distance on the dispersion error. From (2.17) it follows that the numerical group delay error at a distance z is given by

$$\tau_g \equiv \int_0^z \frac{dz'}{v_g(z')} - \int_0^z \frac{dz'}{c(z')} \simeq \frac{1}{8}\frac{z}{c}\Omega^2(\gamma^{-2} - 1), \tag{3.3}$$

where the second expression follows from the approximation in (2.17). For a pulse of length T and upper frequency $\omega_{\max} = 2\pi/T$, it is now required that

$$\frac{1}{8}(2\pi\,\Delta t/T)^2(\gamma^{-2} - 1) \ll \left(\frac{z}{cT}\right)^{-1}. \tag{3.4}$$

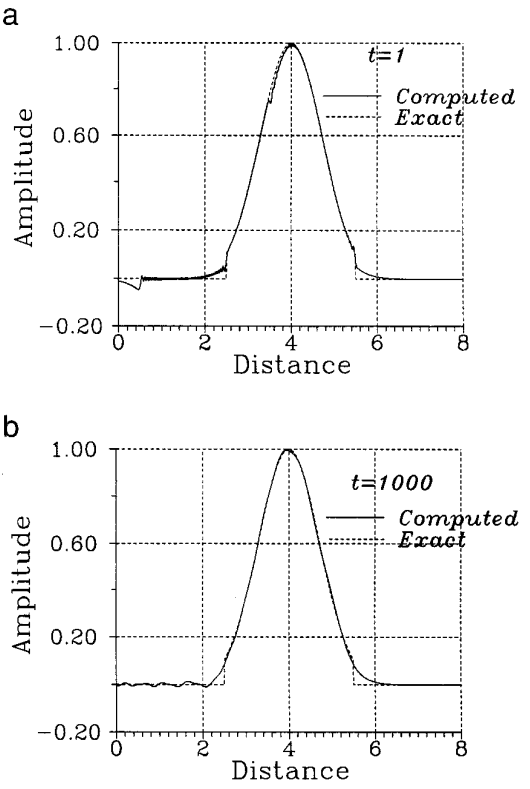

FIG. 6. Evolution of the numerical dispersion error for a truncated Gaussian pulse. Discretization parameters: $\gamma = 0.5$, $\Delta z = 0.005$. (a) $t = 1$. (b) $t = 1000$.

This equation clearly demonstrates how the sampling rate $\Delta t/T$ must be refined as the propagation distance z/cT increases.

The CFL limit $\gamma \to 1$, although desirable from the numerical dispersion standpoint, can cause stability problems in the Eulerian approach. However, when $\gamma < 1$, numerical dispersion will occur. To demonstrate this effect, we considered the propagation of the truncated Gaussian pulse shown in Fig. 6. The numerical result is compared to the exact solution for $t = 1$ in Fig. 6a and for $t = 1000$ in Fig. 6b when the parameters are chosen to be $\gamma = 0.5$ and $\Delta z = 0.005$. The high frequency components observed in Fig. 6a are generated by the discontinuity at the head of the pulse and tend to trail behind it as time increases. Thus, they are first observed within the pulse itself and then appear later at its tail. These higher frequencies exit the window as time progresses; and as a result, the frequency of these numerical noise oscillations decreases. A smoothed pulse is left behind which is compatible with the finite grid. Absorbing boundary conditions (which are the exact one-way wave equation conditions) allow for the trailing components to exit the window without corrupting the remaining pulse. Due to the movement of the window, this error therefore does not interfere with the main pulse. Usage of nonideal boundary conditions would obviously cause local errors at the trailing boundary.

Next, the Euler and the Lagrange formulations are compared, starting with

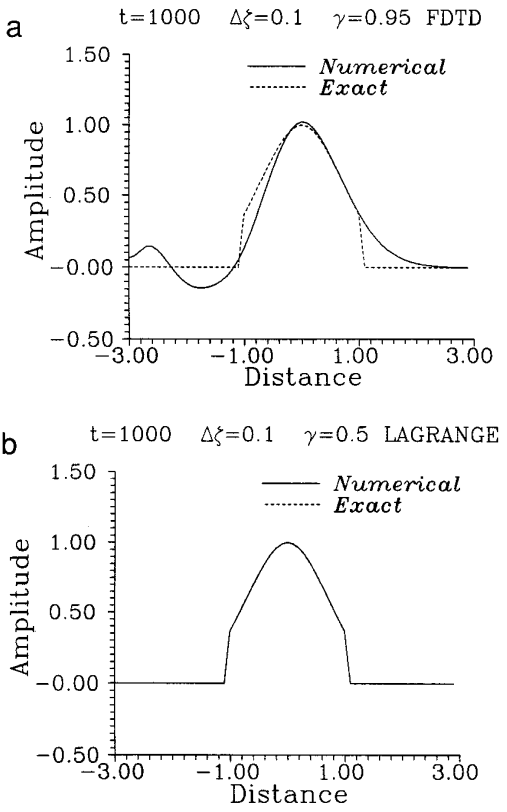

FIG. 7. Comparison of Euler (a) and Lagrange (b) formulation solutions for long range ($t = 1000$) truncated Gaussian pulse propagation in a homogeneous medium. $\gamma = 0.95$ and $\gamma = 0.5$ for the Euler and Lagrange cases, respectively, while $\Delta\zeta = 0.1$ for both cases.

pulse propagation in a uniform medium. The fact that the Lagrange formulation is numerical dispersion free is demonstrated in Fig. 7 for the propagation of a truncated Gaussian pulse. The large error generated by the Euler approach (Fig. 7a) is readily contrasted with the zero error obtained with the Langrange approach (Fig. 7b). To quantify further the errors, we compare in Fig. 8, on an enlarged scale, the errors incurred by the Euler and the Lagrange formulation solutions for long range propagation of a Gaussian pulse. The numerical results are shown for each formulation for two discretization values: $\Delta z = 0.1$ and $\Delta z = 0.01$. As expected, the numerical dispersion error of the Euler formulation solution is smaller for the smaller Δz case. For the Lagrange formulation, no error is observed on the scale of the figure for either of the values of Δz used.

We next compare the Euler and the Lagrange formulations using the optical path length coordinate approach for the case of a Gaussian pulse propagating in a slowly varying medium with the linear velocity profile $c(z) = 1 + 0.004z$. As discussed in Section II.B, the optical path length coordinate approach in the Euler formulation has enabled us to specify $\gamma = 1$ throughout the medium and thereby reduce the numerical dispersion. For the Lagrange formulation we used $\gamma = 0.5$

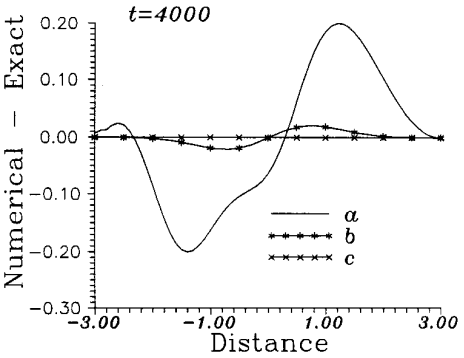

FIG. 8. Comparison of Euler and Lagrange formulation solutions for long range ($t = 4000$) Gaussian pulse propagation in a homogeneous medium. The figure depicts the difference of the numerical solution from the exact (Gaussian) solution. Lines (a) and (b): Euler formulation solutions with $\Delta z = 0.1$ and 0.01, respectively. In both cases $\gamma = 0.98$. Line (c): Lagrange formulation solutions for both $\Delta z = 0.1$ and 0.01 with $\gamma = 0.49$ (they are indistinguishable within the figure scale).

(see Sect. II.C). For each case we used both the discretization $\Delta\zeta = 0.1$ and 0.01. The results of all four cases after a very long propagation time $t = 1000$ are compared in Fig. 9 with the WKB solution

$$E(z, t) = \sqrt{c(z)/c_0} f[t - \zeta(z)/c_0]. \tag{3.5}$$

Notice from the WKB solution that both the amplitude and width of the pulse will

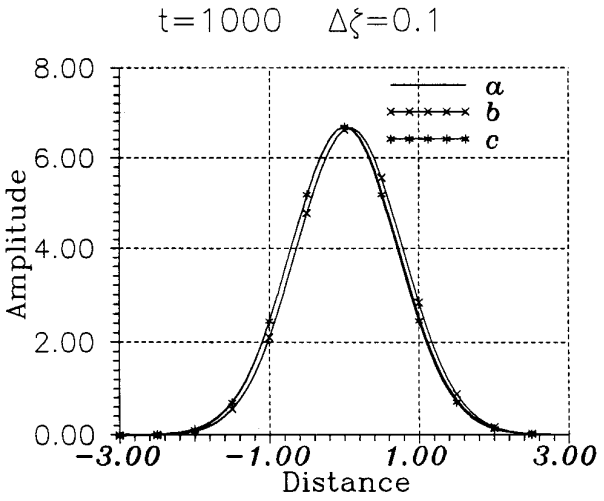

FIG. 9. Comparison of Euler and Lagrange formulation solutions for long range pulse propagation in an inhomogeneous velocity profile: $c(z) = 1 + 0.004z$. Observation time: $t = 1000$. Four different sets of parameters are shown: $\gamma = 1$ and 0.5 for the Euler and Lagrange formulations, respectively. For each case both $\Delta\zeta = 0.1$ and 0.01 are used. Line (a): WKB solution. Line (b): Eulerian solution with $\Delta\zeta = 0.1$. Line (c): The Eulerian solution with $\Delta\zeta = 0.01$ and both Lagrange solutions (they are indistinguishable within the figure scale).

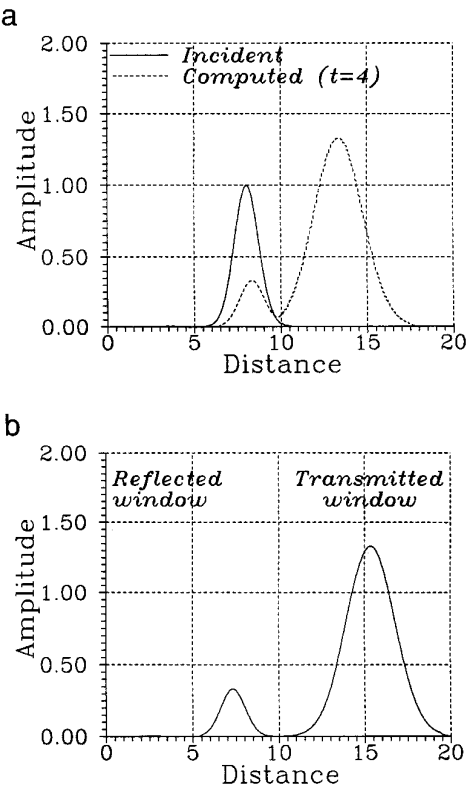

FIG. 10. Interaction of a pulse with an interface. The window attached to the solid line incident pulse in (a) becomes stationary and expands to include both reflected and transmitted pulses near the interface. In (b), the window splits into two windows tracking the two individual pulses.

increase along z as z increases. Except for the Euler formulation with the coarse grid ($\Delta\zeta = 0.1$), all the numerical results coincide with the WKB solution within the scale of Fig. 9.

The interaction of a pulse with a velocity discontinuity causes the pulse to split into reflected and transmitted pulses. These reflected and transmitted pulses are then followed numerically within their own respective windows. The numerical process for modeling the interaction of the incident pulse with this discontinuity begins with "freezing" the window as it intercepts the interface, allowing the incident pulse to split about the discontinuity. The time at which the window was frozen was simply determined by analytically derived times of propagation for the pulse. Ample time for the reflected and transmitted pulses to form was allotted before the reflected and transmitted pulse windows were allowed to propagate. The incident pulse and the numerical solution in this frozen window are shown in Fig. 10a for $t = 4$ from the initial time of incidence of the peak of the incident pulse. At this time the incident pulse has interacted with the interface, but the reflected and transmitted pulses are not yet distinct quantities. After the two distinct reflected and pulses have been formed, this stationary window is split into transmitted and reflected windows, propagating with their respective speeds. The numerical solutions

in each of these oppositely propagating windows are shown in Fig. 10b for the time $t = 5$. Results for both the reflected and transmitted pulses reproduce the exact solution to within a 1% error.

IV. PRELIMINARY EXTENSIONS TO HIGHER DIMENSIONS

Based on the one-dimensional scheme described above, we have extended our results to higher dimensions. In [6], the case of a pulsed beam propagating along a curved trajectory in a two-dimensional space was treated in the following two ways: In the first one, the trajectory was determined *a priori* by ray-optical considerations, and the moving frame orientation was adjusted to follow the curvature of the ray. The second approach involved a real-time calculation of the principal direction of propagation and a subsequent adjustment of the moving frame orientation. The Lagrange formulation was used to calculate the field in the moving frame. The pulsed beam is characterized by a narrow angular spectrum centered about the principal direction of propagation. Therefore, the dispersion characteristics of this higher dimensional Lagrange case are similar to those of the one-dimensional case discussed above. The numerical results indeed exhibit very low numerical dispersion errors, and they follow the analytical results very closely.

In [7], the method was further extended to 2.5 dimensions to model the propagation of an axially symmetric pulsed beam in both a stratified medium and a parabolically graded index waveguide. The one-dimensional numerical dispersion and stability analysis have been extended to these 2.5 dimensional cases. Again, the benefit of very low numerical dispersion errors has enabled the simulator to produce accurate results over the order of 10^5 time steps, which is the equivalent of the order of 10^3 pulse lengths. The issue of formulating the appropriate boundary conditions was recognized as critical, and has also been addressed in [7].

V. CONCLUSIONS

In this paper we introduced several numerical schemes that can be used to simulate the propagation of electromagnetic pulses in homogeneous and inhomogeneous media over very large distances (thousands of pulse lengths). The main idea is a moving window approach. Both Eulerian (a moving window in a stationary coordinate frame and a moving window in a speed-normalized coordinate frame) and Lagrangian (a window in a propagating frame of reference) approaches were considered. Stability and numerical dispersion analyses for all of these approaches were established with a similar procedure, and their implications were discussed. These derivations of the numerical stability and dispersion relations properly take into account either abrupt or slowly varying inhomogeneities in the medium; a successive approximation version of these derivations could be used to quantify the higher order corrections to these relations. Scattering from interfaces (abrupt discontinuities in the medium properties) was also considered.

In the Eulerian approach a speed-normalized transformation was used to optimize the discretization for the desired long range propagation distances. This transforma-

tion allowed $\gamma \to 1$ and provided a constant numerical group velocity. It can be viewed as nonuniform sampling with constant delay sampling instead of uniform Δz sampling (such a discretized approach is termed the Goupillaud layered medium [5]).

In the Lagrange approach it was shown that in the moving coordinate frame there is no numerical dispersion for the forward moving part of the solution, but twice as large numerical dispersion for the backward propagating part. Since that backward propagating part leaves the moving window without generating any numerical noise, the forward propagating pulse is very accurately modeled with this scheme over extremely large propagation distances. The only penalty for this dispersion-free numerical propagation is that the resulting CFL condition must take into account the largest velocity in the frame, i.e., the backward velocity $-2c(z)$. The resulting extra number of timesteps in any given simulation is a small addition in simulation cost in comparison to the added costs that would be incurred in the Eulerian approach if the discretization grid would be refined in order to reduce the numerical dispersion to an acceptable level or if the entire propagation range had to be gridded.

When interfaces are involved, the moving window approaches must be modified slightly. We introduced a scheme that uses a frozen window when the propagating pulse begins to interact with the interface. The window is frozen until the reflected and transmitted pulses are fully generated, and then moving windows are assigned to the resulting reflected and transmitted pulses. Propagation of those pulses is simulated by following moving windows in each of their respective media.

Several comparisons of the numerical results generated by the Eulerian and Lagrangian approaches were made for pulses propagating in homogeneous and inhomogeneous media. An interface example was also treated. The numerical dispersion errors and the overall simulation accuracies of these schemes were quantified with these validation cases; the results were checked against the analytically derived estimates. Excellent agreement with the exact or known WKB solutions was found in all cases with the Lagrangian simulator. It was shown how even the Eulerian approach could be used to generate reasonable results with appropriate choices of the discretization parameters.

Because these one spatial dimension results were so promising, we have extended them to higher dimensional geometries, as alluded to in Section IV. The higher dimensional cases that have been treated with our moving frame approach, will be summarized in detail in a forthcoming paper. We are also beginning to apply our results to microwave and optical pulse propagation in complex media for a variety of remote sensing and communications applications. We will begin to include material dispersion and nonlinearities as our approach is applied to yet more complex problems.

ACKNOWLEDGMENT

This work is supported by the US–Israel Binational Science Foundation, Jerusalem, Israel, under Grant 92-00273.

REFERENCES

1. E. Heyman, Pulsed beam propagation in inhomogeneous medium, *IEEE Trans. Antennas Propagat.* **AP-42,** No. 3, 311 (1994).
2. K. Yee, Numerical solution of initial boundary value problems involving Maxwell's equations in isotropic media, *IEEE Trans. Antennas Propagat.* **AP-14,** No. 3, 302 (1966).
3. K. S. Kunz and R. J. Luebbers, *Finite Difference Time Domain Method for Electromagnetics* (CRS Press, Boca Raton, 1993).
4. D. Potter, *Computational Physics* (Wiley, New York, 1973).
5. P. L. Goupillaud, *Geophys.* **26**(6), 754 (1961).
6. E. Aloni, R. Kastner, E. Heyman, and R. W. Ziolkowski, Reduction of numerical dispersion errors in the FDTD with multiple moving coordinate systems, in *Proc. 1996 URSI National Radio Science Meeting, Baltimore, MD, July 21–26, 1996.*
7. Y. Pemper, B. Fidel, E. Heyman, R. Kastner, and R. W. Ziolkowski, Absorbing boundary conditions in the context of the hybrid ray–FDTD moving window solution, in *Proc. 1997 IEEE AP-S International Symposium, Montreal, PQ, Canada, July 14–19, 1997.*